Chapter 4: *Local Weather* - Lead Author D J Parker

In this chapter we consider a set of challenges in weather forecasting for specific geographic locations, such as a particular village, town or airport. We consider phenomena on timescales from a few hours to one to two days, within which such localised forecasts are needed. The weather phenomena to be considered all tend to be linked, scientifically, through the dynamics of the planetary boundary layer (PBL), and are influenced by the local topography of hills, coastlines and land cover, on scales of a few tens of kilometres or even less – known as the mesoscale. This chapter is concerned therefore with predicting a family of weather patterns within the general areas of mesoscale and boundary-layer meteorology. We will not here discuss rainfall prediction in great detail, as this aspect is covered in Chapters 2, 3 and 6. However, initiation of local showers will be discussed.

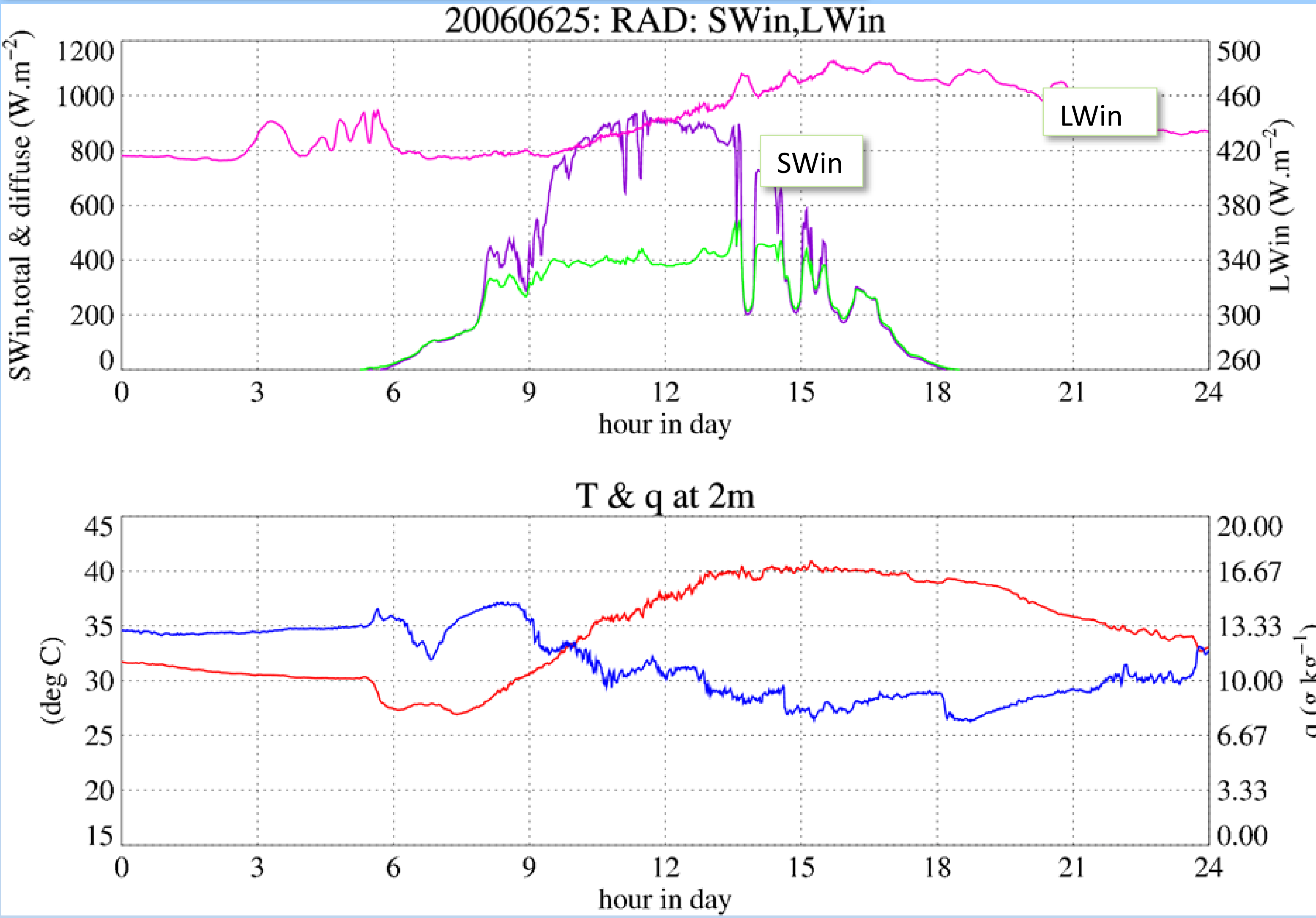

Figure 4.1: A typical diurnal cycle of the surface energy balance, with 2 m temperature and specific humidity at Niamey, taken from the ARM Mobile Facility during the AMMA campaign, 25 June 2006.

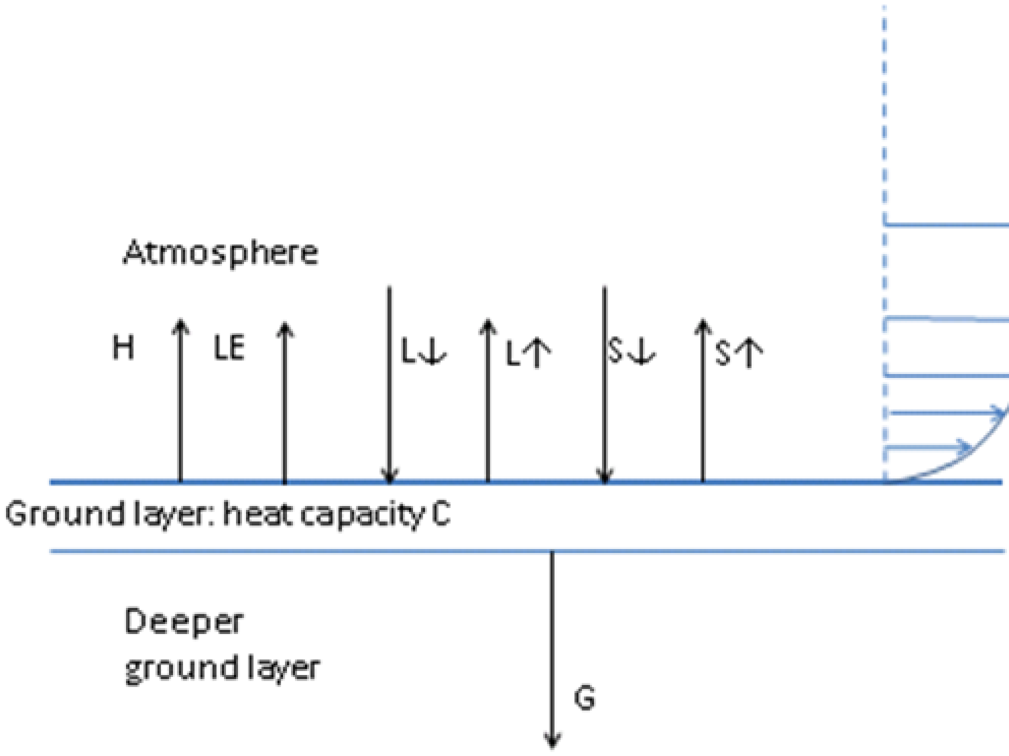

Figure 4.2: Schematic of surface energy balance terms used in (4.8), and the typical surface wind profile.

Note that in the surface layer, the mean wind direction is approximately constant with height.

Greater diurnal cycle at drier sites Agadez, Niamey, black and red) in June.

August: Niamey (red) is more humid and diurnal cycle reduces.

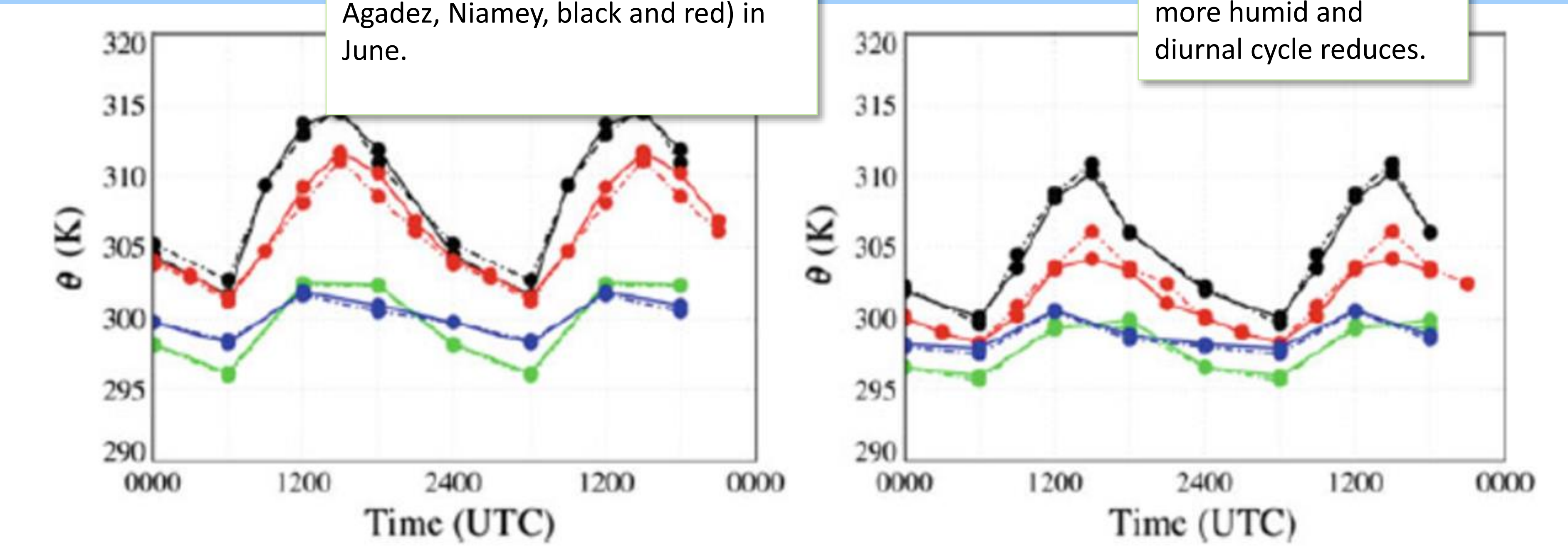

Figure 4.3: The diurnal cycle of 2 m potential temperatures for June (left panel) and August (right panel) for the stations at Agadez (black line, 17°N), Niamey (red line, 13.5°N); Parakou (green line, 9.5°N) and Cotonou (blue line, 6.5°N). For clarity two diurnal cycles are shown. Solid lines show data from 2006; dashed lines are for August 2005-2008. From Gounou et al. (2012).

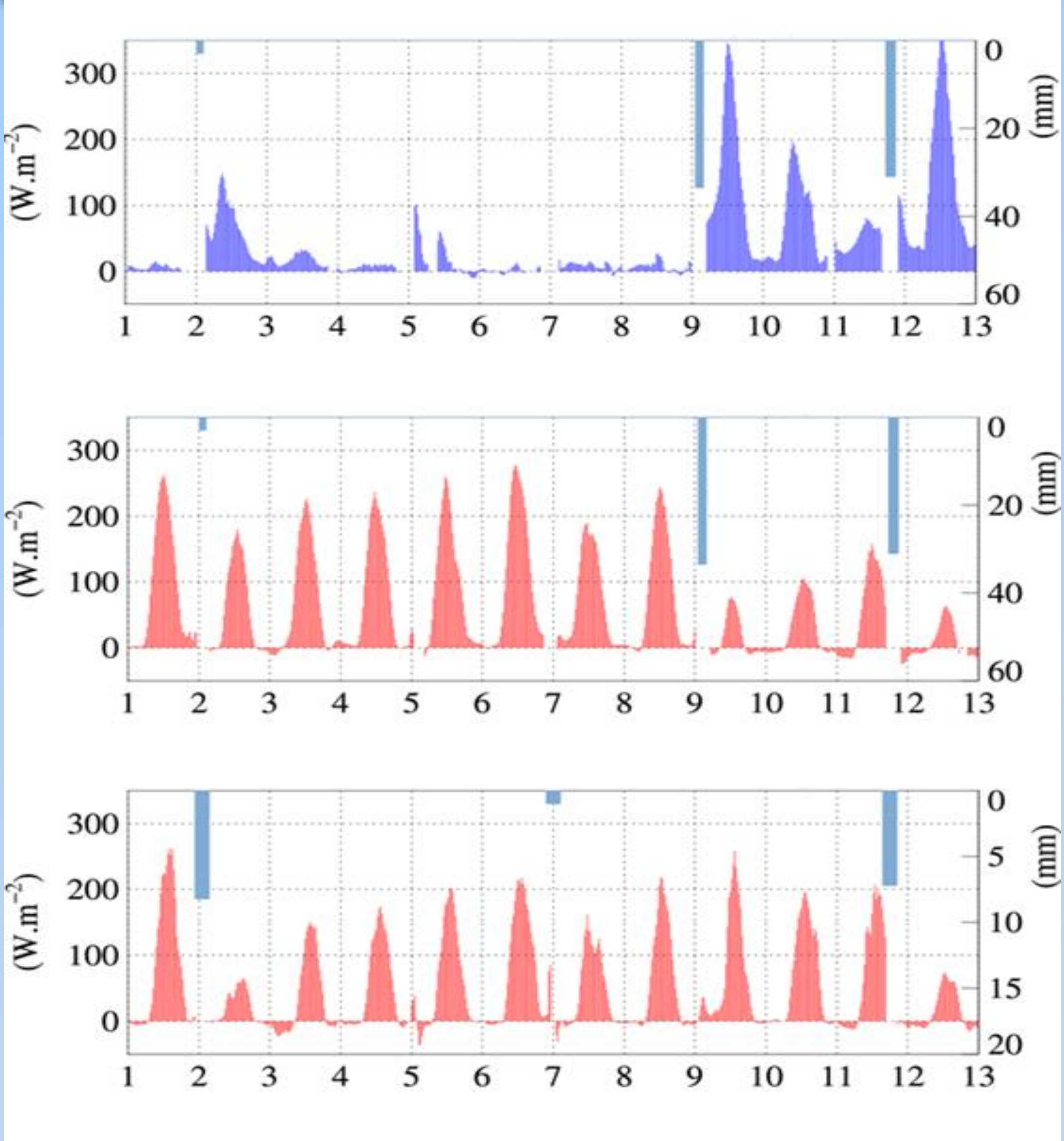

Figure 4.4: Spatio-temporal variability of surface heat fluxes in measurements made in the vicinity of Niamey: the horizontal axis indicates dates in July 2006.

The top two plots show time series of surface latent (blue) and sensible (red) heat fluxes in Wankama, with precipitation events indicated with thick blue bars.

The bottom plot shows the sensible heat fluxes in Banizoumbou, a few tens of kilometres away.

Sensible heat fluxes are reduced, and latent heat fluxes increase, for a few days after rain.

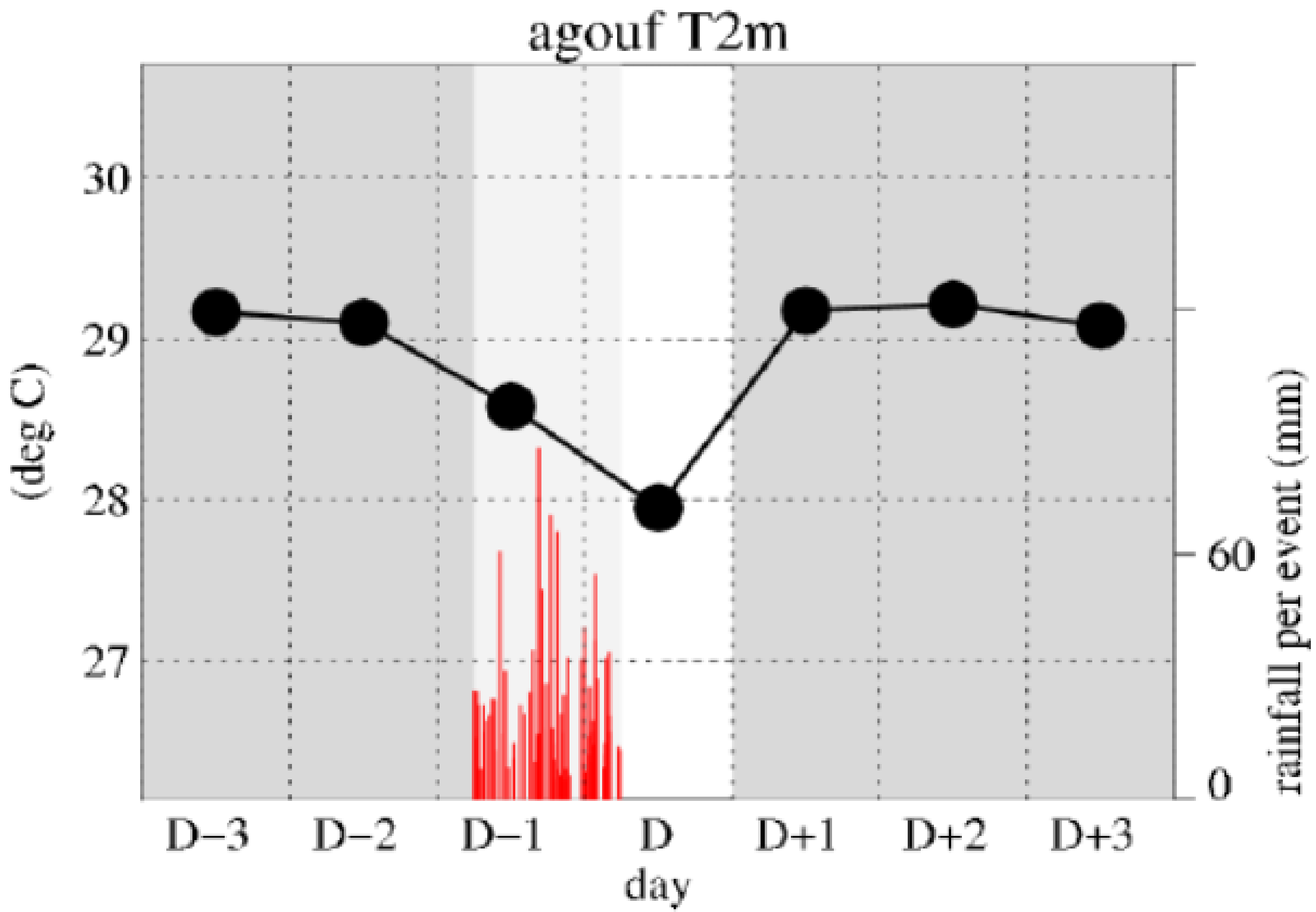

Figure 4.5: Rainfall events (greater than 5 mm) and composite 2 m temperature observations from the Agoufou site (15.3°N, 1.6°W) in the Hombori mesoscale site of the AMMA-CATCH network, in the period 2002 to 2006.

Surface temperature is reduced, for one or two days after rain.

Chapter 4: *Local Weather* - Lead Author D J Parker

Figure 4.6: Photographs of non-precipitating convective clouds: (a) shallow cumulus (cumulus humilis), observed at Niamey; (b) cumulus congestus, observed from the UK BAE146 research aircraft during AMMA, with deeper cumulonimbus in the background; (c) isolated, precipitating cumulus cloud observed in much drier tropospheric conditions near Hombori. Photos: Douglas Parker (a), (b) and Françoise Guichard (c).

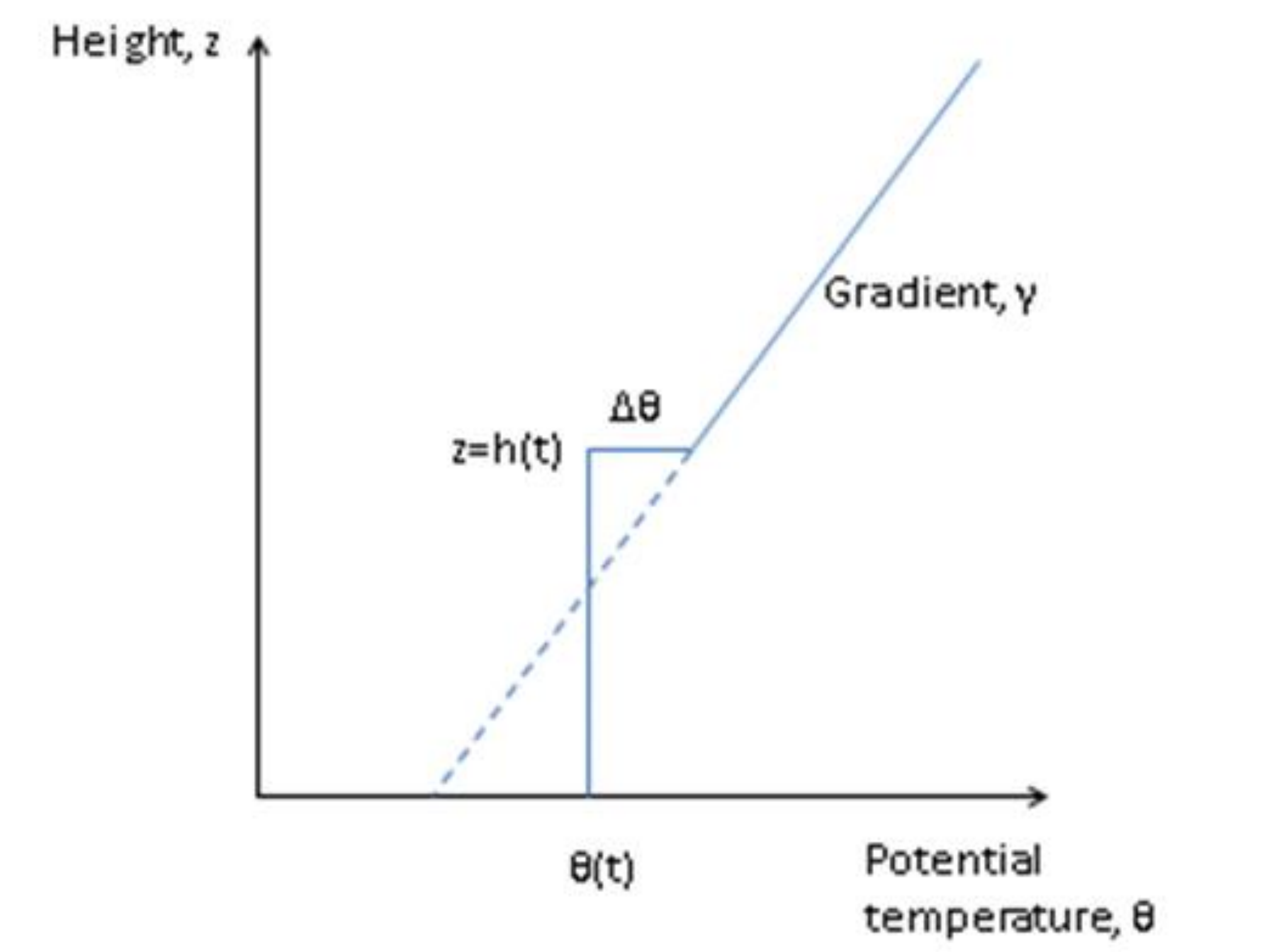

Figure 4.7: Schematic of the bulk boundary layer model yielding (4.12 and 4.13). The well-mixed CBL has constant potential temperature, θ, up to height z=h, and is capped by a jump in θ, at this height, above which there is constant stratification. As the CBL is heated by sensible heat fluxes from the surface, h and θ both increase in time.

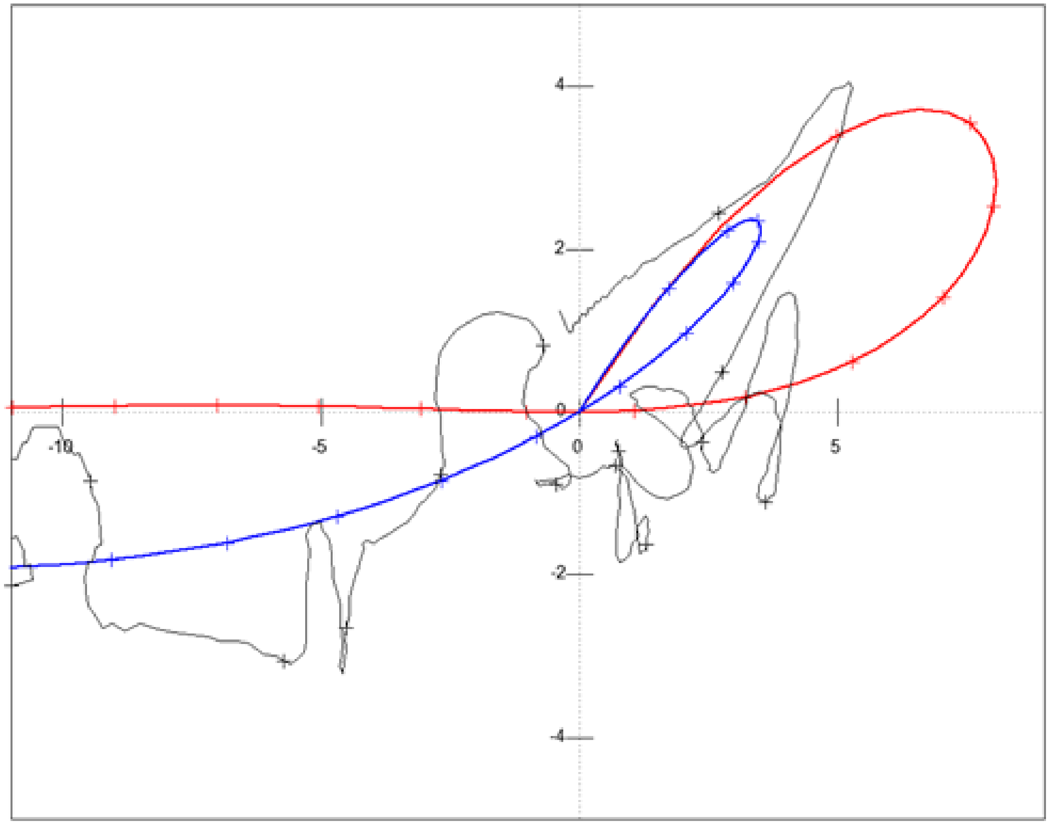

Figure 4.8: Hodograph (locus of the (u,v) wind vector) of the modified Ekman solution, as described by (4.14), with surface geostrophic wind of 15 ms^{-1} westerly, and an AEJ of 15 ms^{-1} at 3 km height. The two curves show solutions with scale-height δ =500 m (red) and 1500 m (blue). Both solutions have (u,v)=0 at the surface, by definition, and the crosses mark heights at 200 m intervals above the surface. The thin black line shows the hodograph for the Niamey sounding at 1200 UTC on 21 June 2006

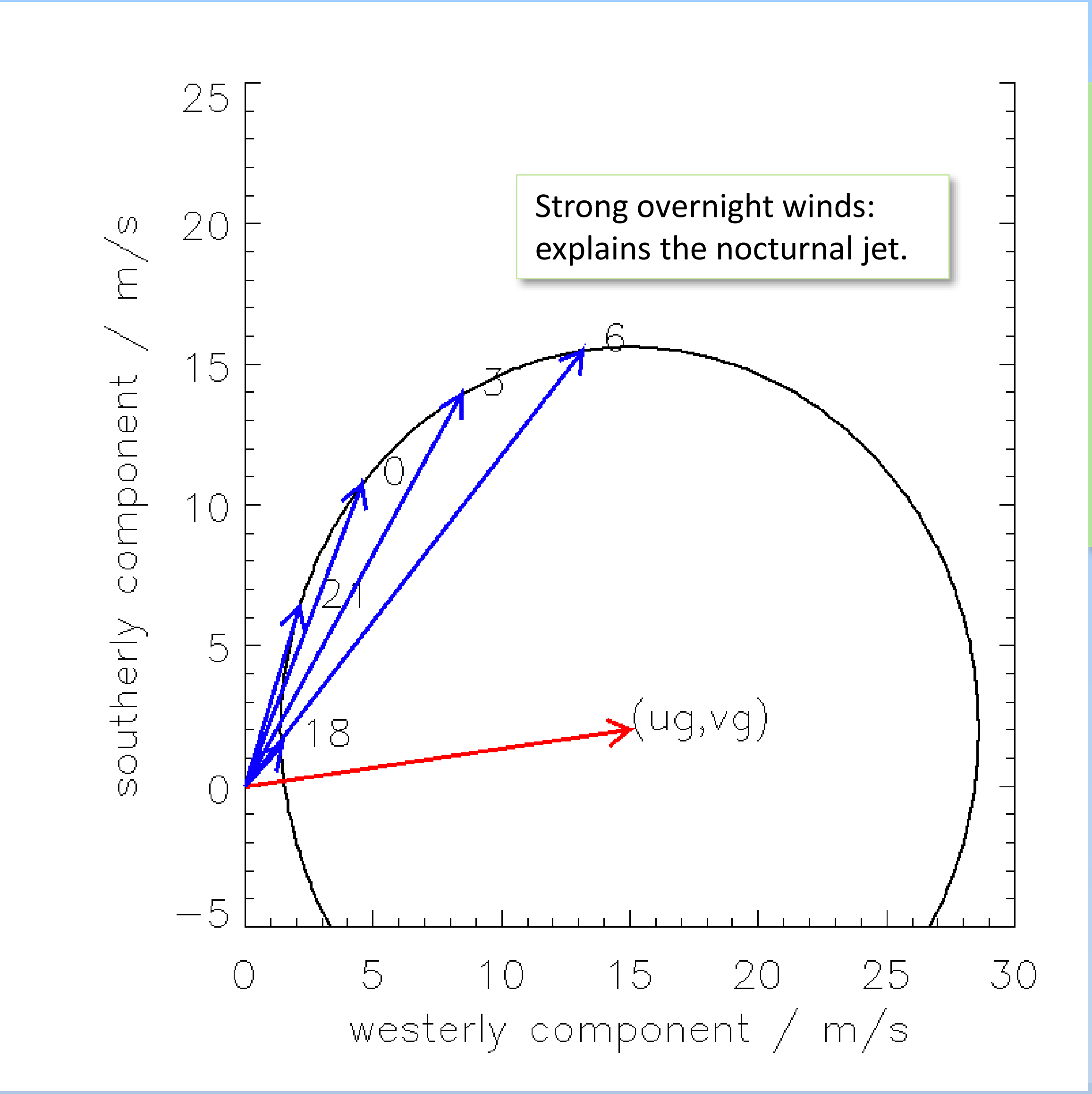

Figure 4.9:(a) Hodograph of (u,v) vectors, showing an example of the solution of equation (4.19) for an inertial oscillation in the nocturnal winds, indicating the wind vectors (blue) at 2-hourly intervals (labelled in local time), assuming the oscillation starts at 1800 UTC. The geostrophic wind vector is shown in red.

Table 4 Characteristics of the low-level nocturnal jet during SOP-1 and SOP-2: frequency of occurrence, averaged maximum speed and altitude

	SOP-1			SOP-2		
	Freq (%)	Speed (m s^{-1})	Altitude (m)	Freq (%)	Speed (m s^{-1})	Altitude (m)
Agadez	35	9.9 (5.9–15.2)	230 (110–370)	80	9.4 (5.2–17.0)	260 (130–670)
Niamey	60	10.9 (5.1–19.0)	320 (90–670)	85	8.5 (5.2–15.6)	360 (170–730)
Parakou	55	8.6 (5.3–19.3)	300 (130–590)	50	8.1 (6.0–12.0)	255 (110–430)

The minimum and maximum values are indicated in brackets

Table 4.1: Jet maxima and altitudes at different stations according to season. SOP-1 is the pre-monsoon period, May to June 2006, and SOP-2 is the full monsoon period of July to August. From Gounou et al. (2012).

African Monsoon Multidisciplinary Analysis

ACMAD

WMO

Chapter 4: *Local Weather* - Lead Author D J Parker

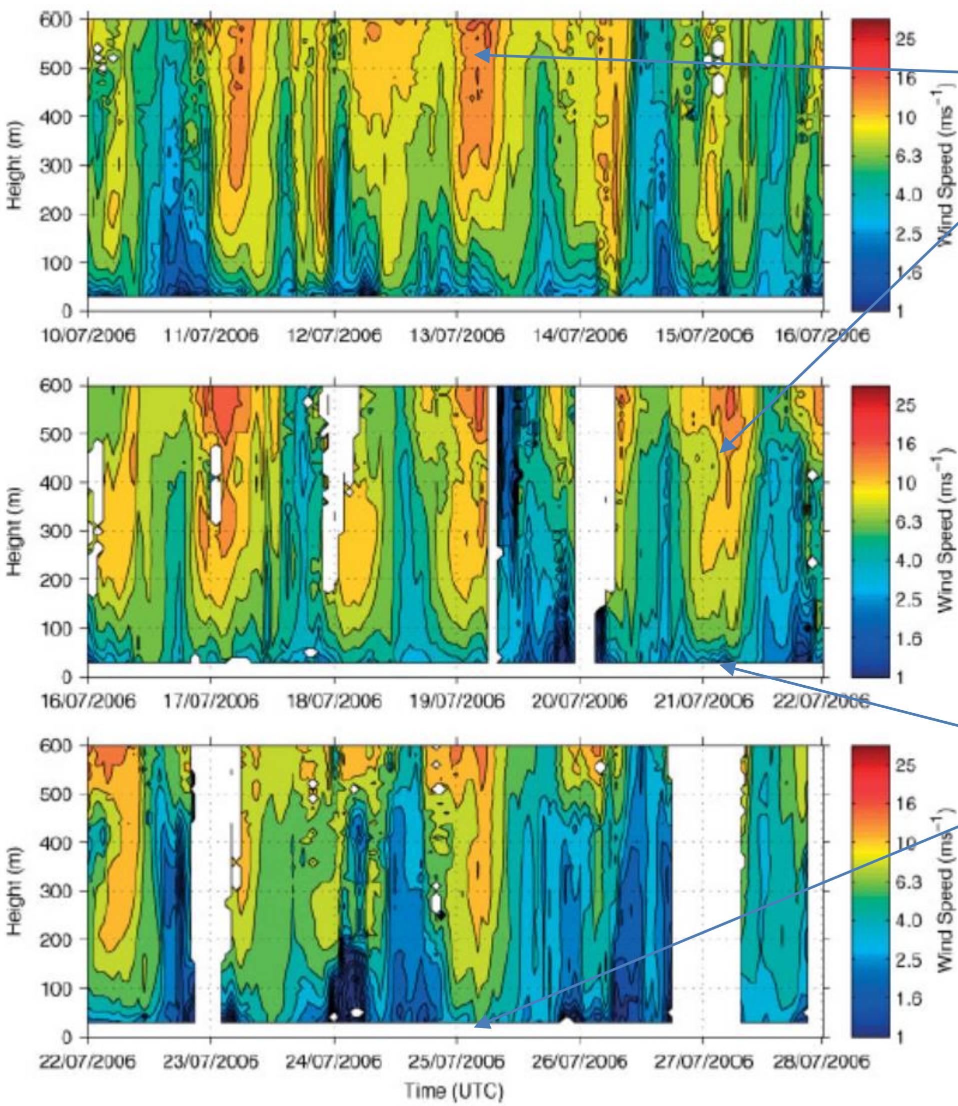

Nocturnal jets in wind-speed around Niamey, almost every night.

Figure 4.10 (From Abdou et al., 2010): Time-height contours of wind speed, averaged over a set of 4 sodars deployed around Niamey, in the period 10 to 27 July 2006.

High winds are mixed down to the surface in the morning.

African Monsoon Multidisciplinary Analysis

ACMAD

WMO

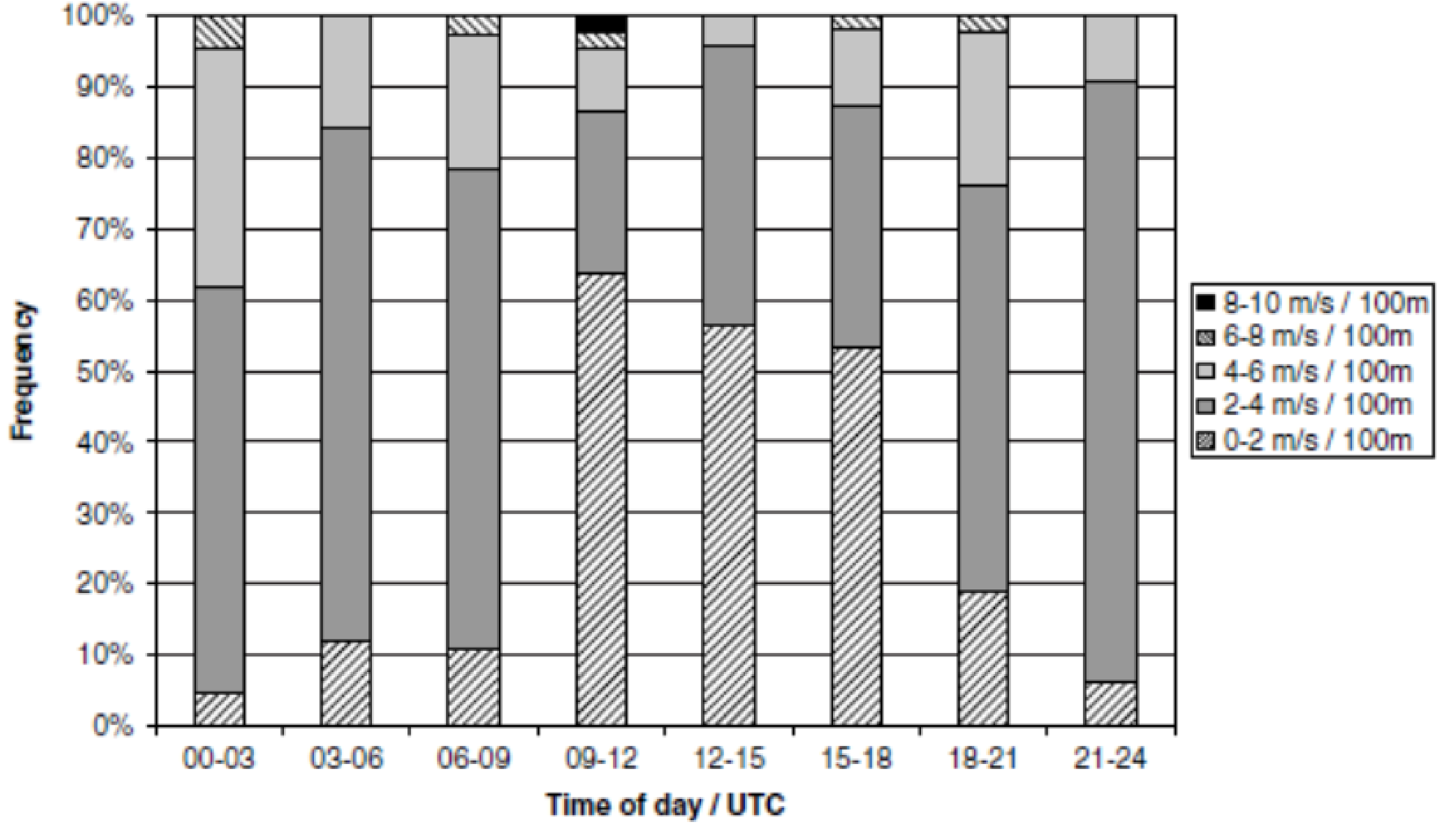

Figure 4.11 Frequencies of most intense 15-minute wind-shears from a set of sodars deployed for the AMMA SOPs in the Niamey region in July to August 2006. The central category, of 4 to 6 ms-1 / 100 m, is the one which would commonly require the notification of high wind-shear to pilots. Note that these observations do not represent a reliable climatology of wind-shear from convective squalls, because the sodars do not sample under conditions of falling precipitation. From Abdou et al., 2010.

Chapter 4: *Local Weather* - Lead Author D J Parker

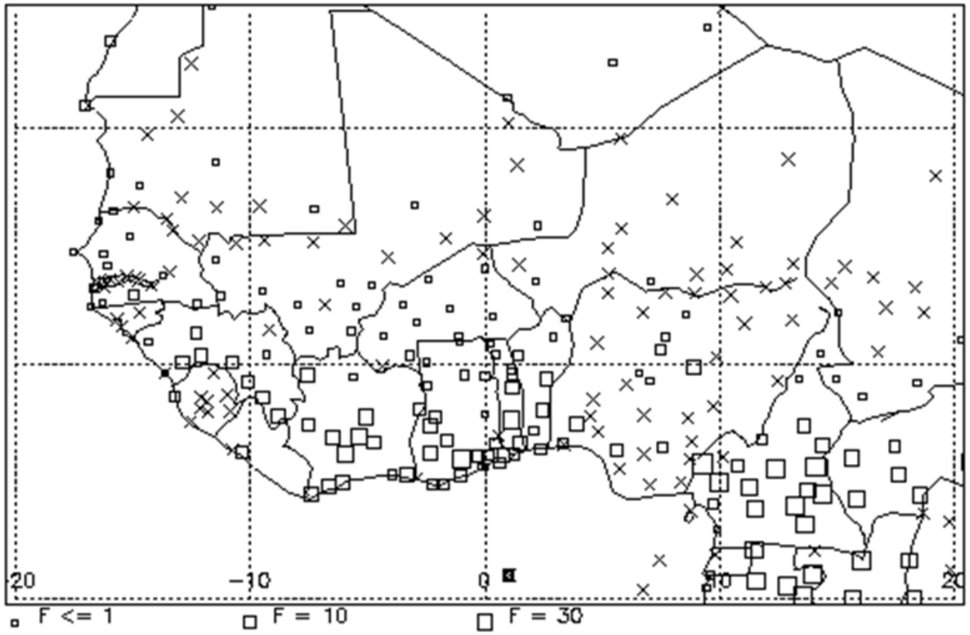

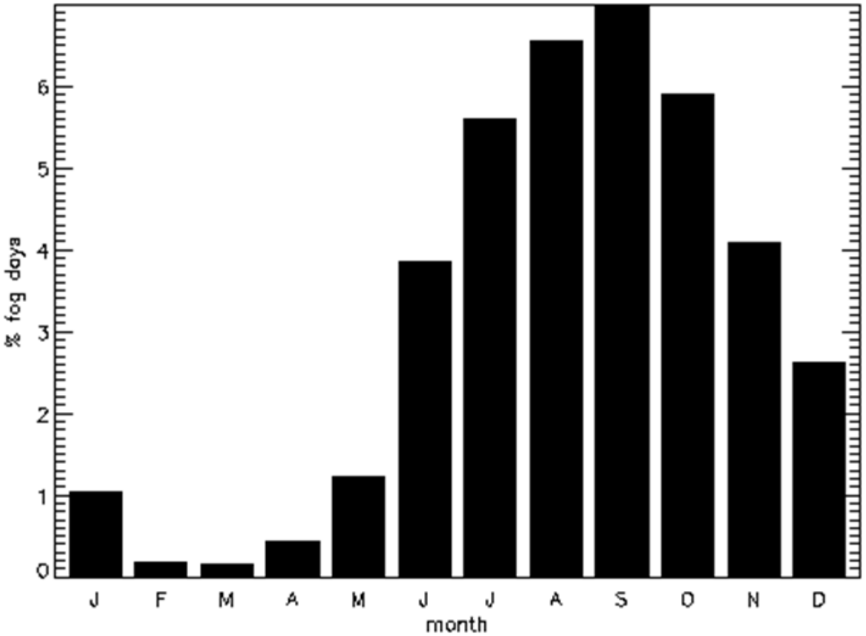

Figure 4.12: Fog Climatology (a) Statistics of 0600 UTC fog reports: numbers denote F , the mean annual frequency of reports of fog at each station, while stations with no reports are marked "x". Some stations with frequencies above F=20 have very low numbers of total reports and may have large errors on the exact value of F, but are retained here to show the geographic coverage of reports. (b) Monthly frequency of fog reports at 0600 UTC, as a percentage of all reports at 0600 UTC, for stations in the geographic zone 10°W to 10°E, 7-10°N. Data are taken from West African synoptic station reports, for the years 1984 to 2012, obtained from the MIDAS database at BADC.

African Monsoon Multidisciplinary Analysis

Figure 4.13: Photograph of fog approaching Takoradi airport, around 1 nautical miles from the sea, on 8 January 2012, 0630 UTC.

Chapter 4: *Local Weather* - Lead Author D J Parker

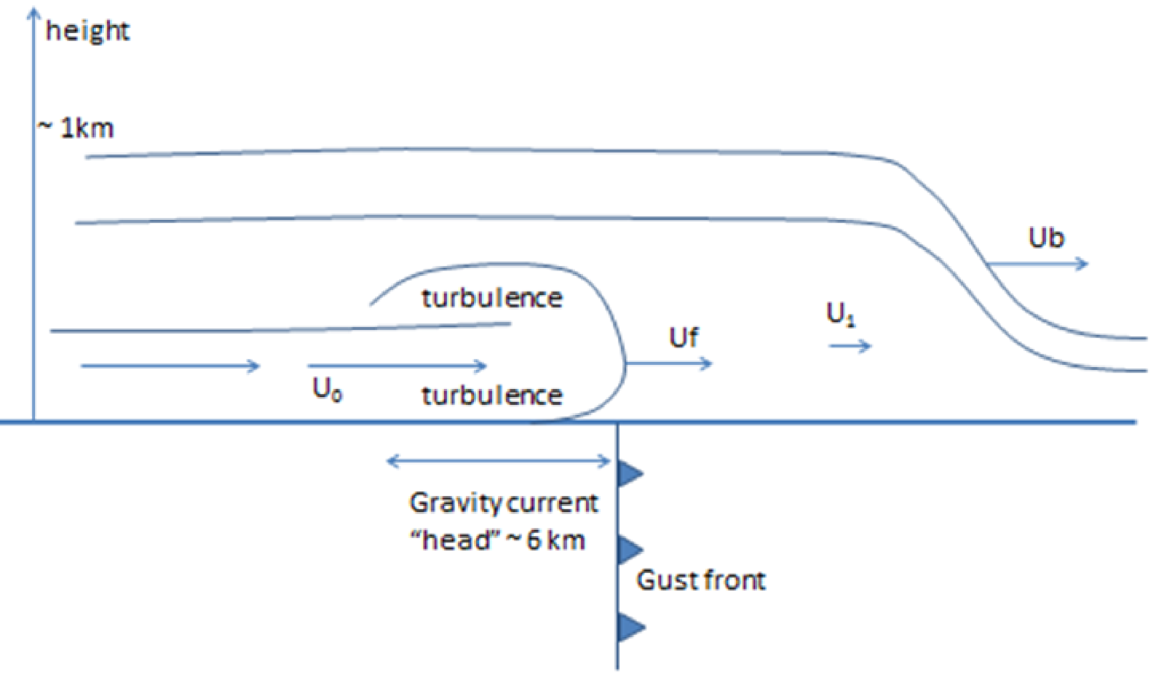

Figure 4.14: Imagined situation of a gravity current penetrating into a nocturnal inversion, with a bore moving ahead of that. The feeder flow for the gravity current has a speed, U0, which is greater than the gravity current speed Uf. In contrast, the speed of the bore, Ub, is greater than the speed of the flow behind it, U1, so the bore moves as a wave through the flow. The excess air moving into the gravity current head is mixed out by strong turbulence in this region, and forms a mixed layer which is left behind the head, above the feeder flow.

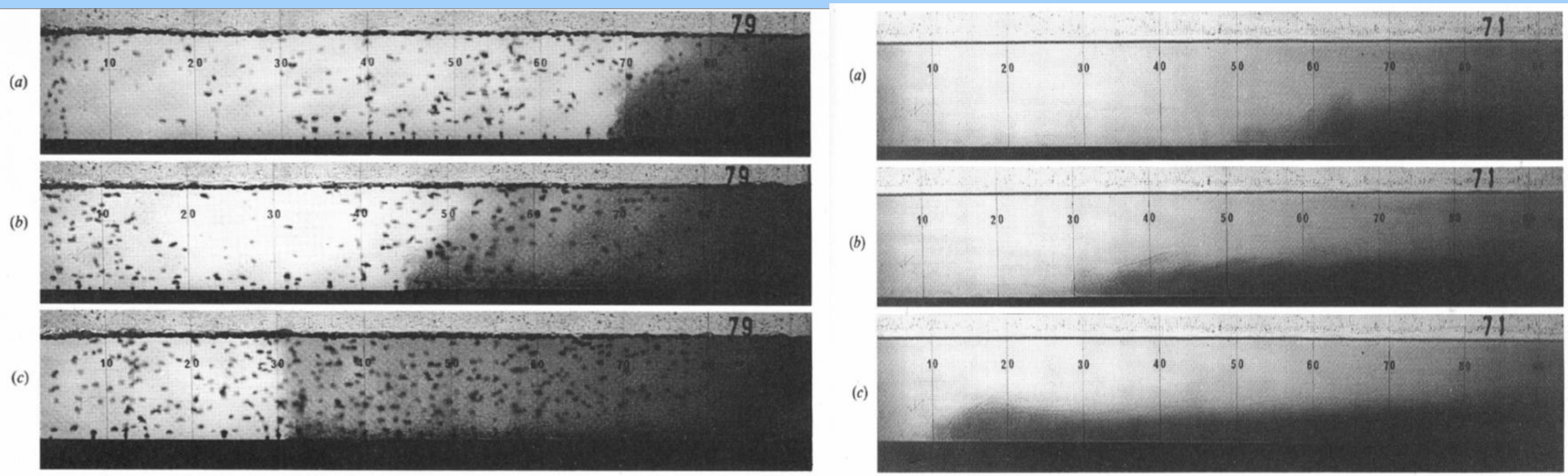

Supporting Figure S4.15: The laboratory fluid dynamics experiments of Linden and Simpson (1989) show how mesoscale density gradients may be sustained in the atmosphere by day and by night. Reproduced from Linden and Simpson (1989)

This is like daytime conditions, with convective turbulence. The mean flow is weak, and the horizontal temperature gradient is sustained.

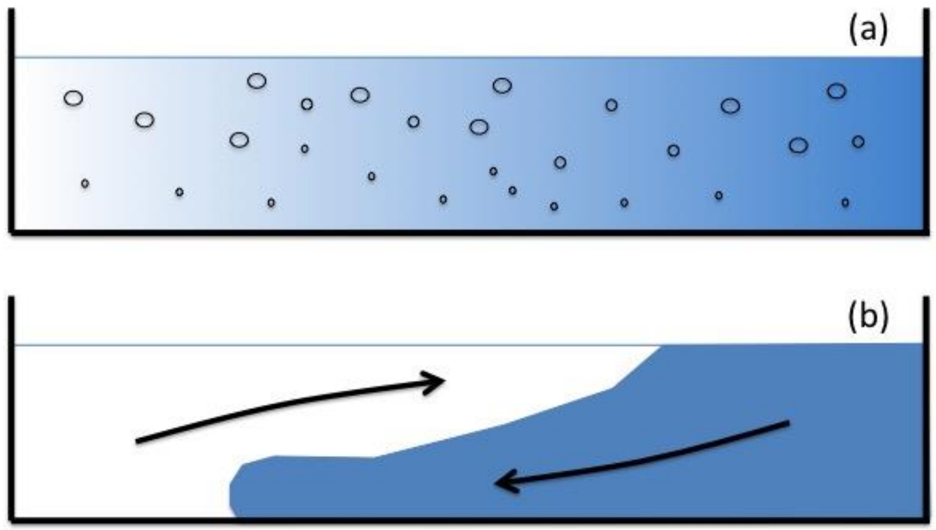

This is like night-time conditions, when convective turbulence has disappeared. The mean flow accelerates, and the horizontal temperature gradient forms a sharp, propagating front.

Figure 4.15: A sketch indicating the general results of the laboratory fluid dynamics experiments of Linden and Simpson (1989), which suggest how mesoscale density gradients may be sustained in the atmosphere by day and by night. The dark fluid is denser than the ambient and represents cold air in the atmosphere. When the flow is turbulent (panel (a)), then a horizontal density gradient can be maintained, with relatively weak horizontal flow. When the turbulence diminishes (in the atmosphere, at night – panel (b)) then the dense fluid slumps below the ambient, in the form of a gravity current.

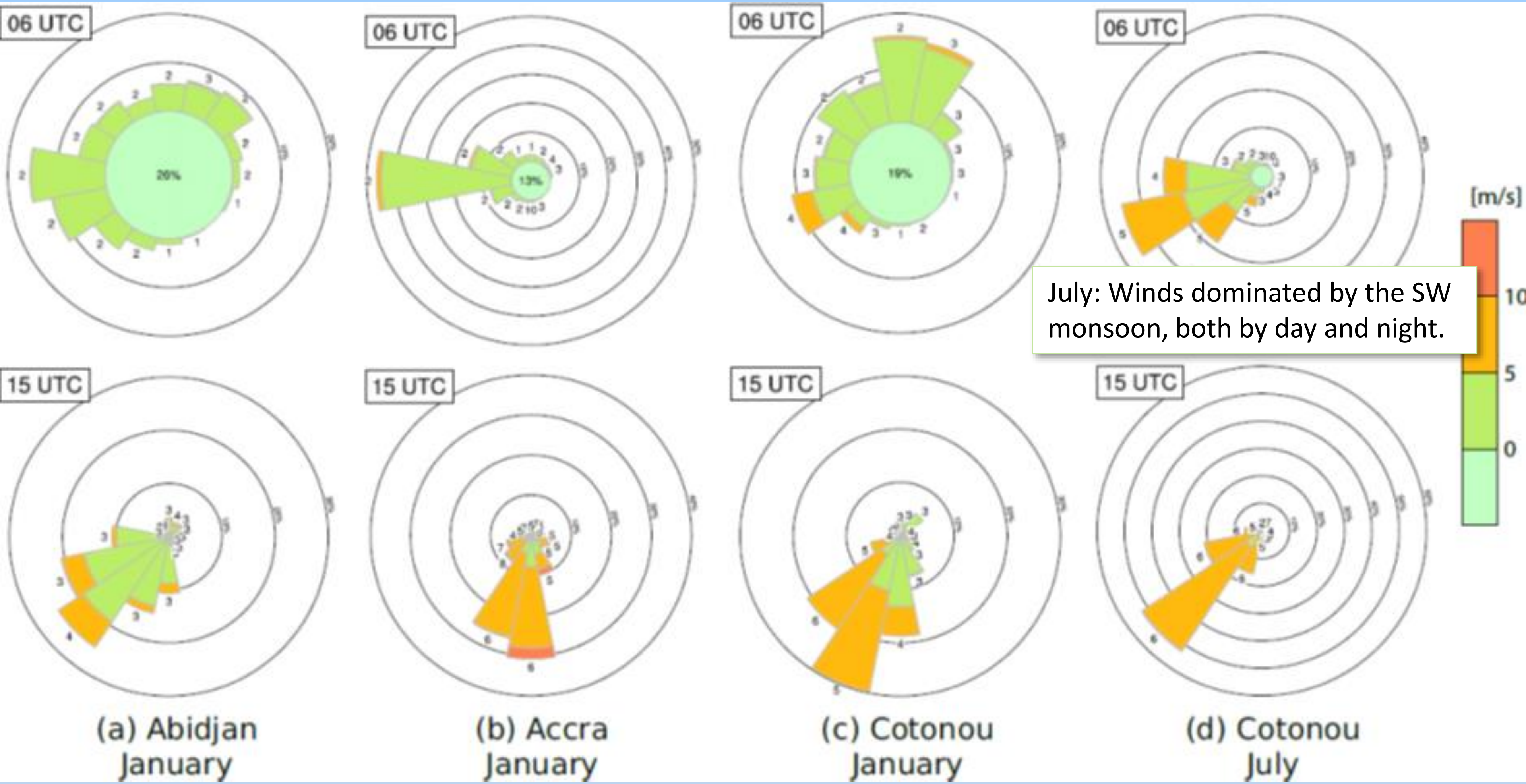

July: Winds dominated by the SW monsoon, both by day and night.

Figure 4.16: Wind roses showing the patterns of land and sea breezes for three stations on the Guinea Coast.

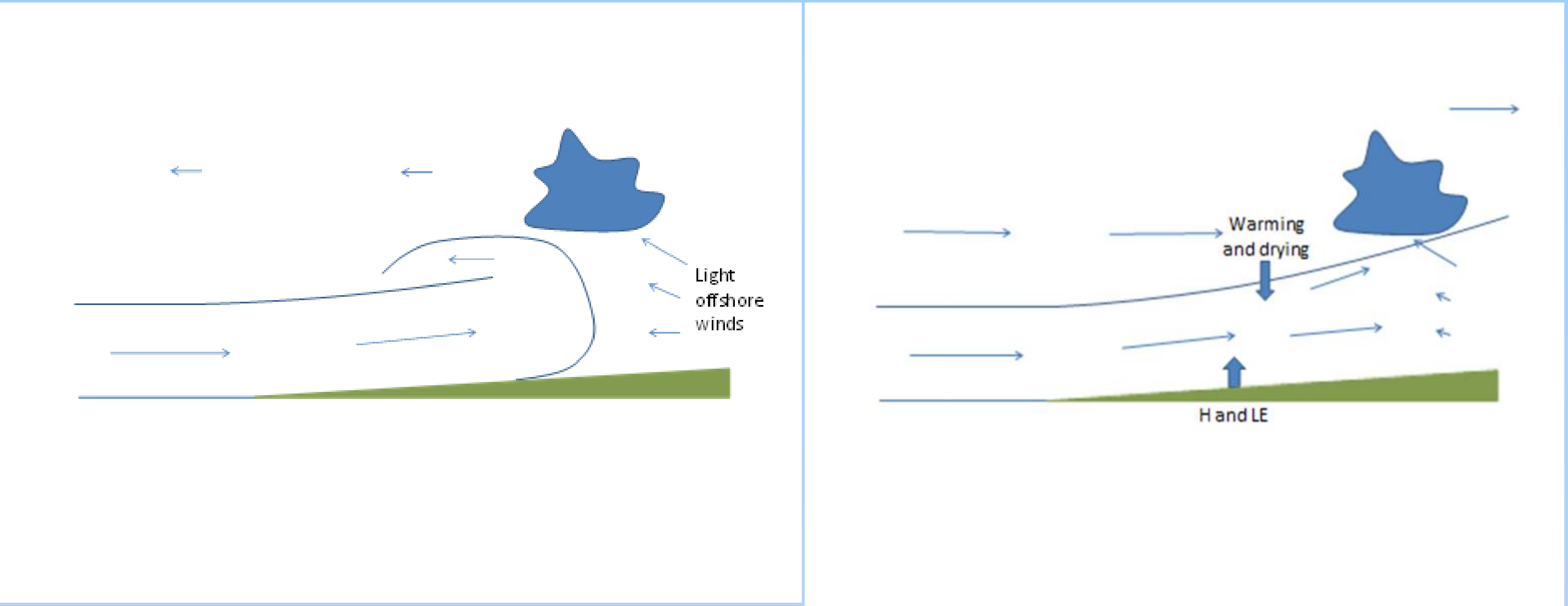

Figure 4.17: Schematics of gravity current / PBL transition models for the sea breeze during the day. In (a) there are light offshore winds and the sea breeze progresses inland as a coherent gravity current, once the thermal contrast between land and sea is established in the morning. In (b) there is a robust onshore wind, as seen on the Guinea Coast when the monsoon is active. There is little diurnal signal in the winds at the coast, but in the morning, as the land warms up and the surface fluxes increase, the maritime boundary layer air is warmed as it moves inland, until cumulus can be formed at some distance inland.

Chapter 4: *Local Weather* - Lead Author D J Parker

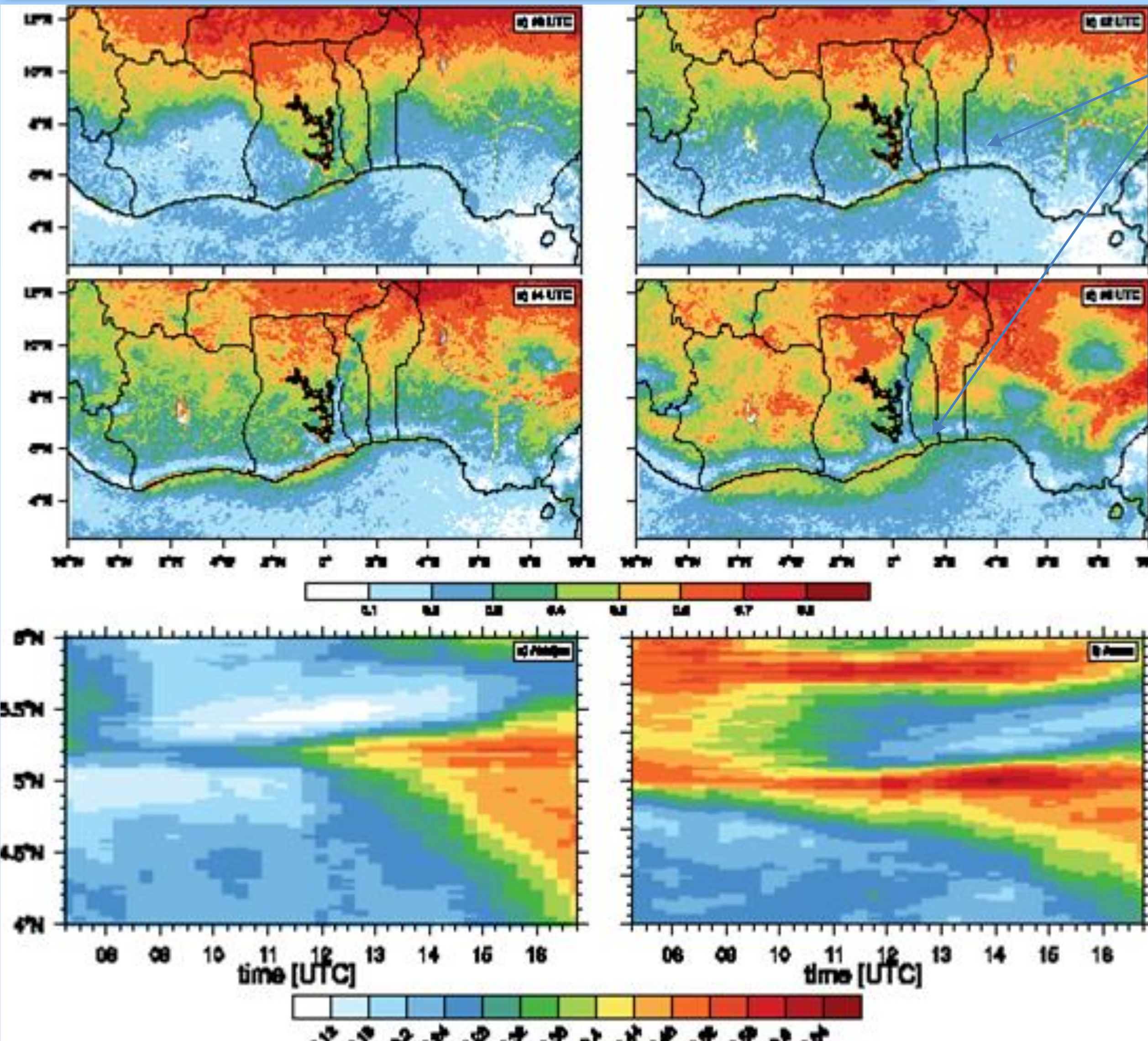

Cloud band (white) develops at the coast and moves inland.

Figure 4.18: Satellite-derived frequency of clear skies at a) 1000 UTC, b) 1200 UTC, c) 1400 UTC, and d) 1600 UTC determined by the SAFNWC cloud type classification for October 2007 to 2011 (Derrien and Le Gléau (2005)).

Red colours show clear skies and the land surface; blue and white colours indicate cloud fields. The final panels show the time-latitude sections of these data, for lines of longitude running through (e) Abidjan and (f) Accra.

The sea breeze has some typical features:

(i) Moderate / fresh wind speeds, typically ~10 kts at Cotonou, with onset at around 1100 to 1400 local time, attaining a maximum speed by early afternoon, and terminating around 2000 local time (Bajamgnigni Gbambie and Steyn, 2013);

(ii) The flow extends vertically to approximately 1 km;

(iii) The flow can penetrate to approximately 100 km inland;

(iv) It develops best during the dry season;

(v) Weak pressure and temperature gradients are in evidence; there is an absence of major synoptic features;

(vi) Light, offshore, ambient winds are present.

The land breeze has some characteristic features:

(i) Weak wind speeds, usually ≤ 5kts;

(ii) Extends just a few hundred metres vertically;

(iii) It is best developed near dawn when the water surface is relatively warm.

Lake breezes may also be significant, for instance in the vicinity of Lake Volta. Vegetation breezes have been shown to exist, in relation to strong contrasts in surface vegetation cover (e.g. from forest to cropland), but these are likely to be relatively weak, of a few kt, and intermittent.

Chapter 4: *Local Weather* - Lead Author D J Parker

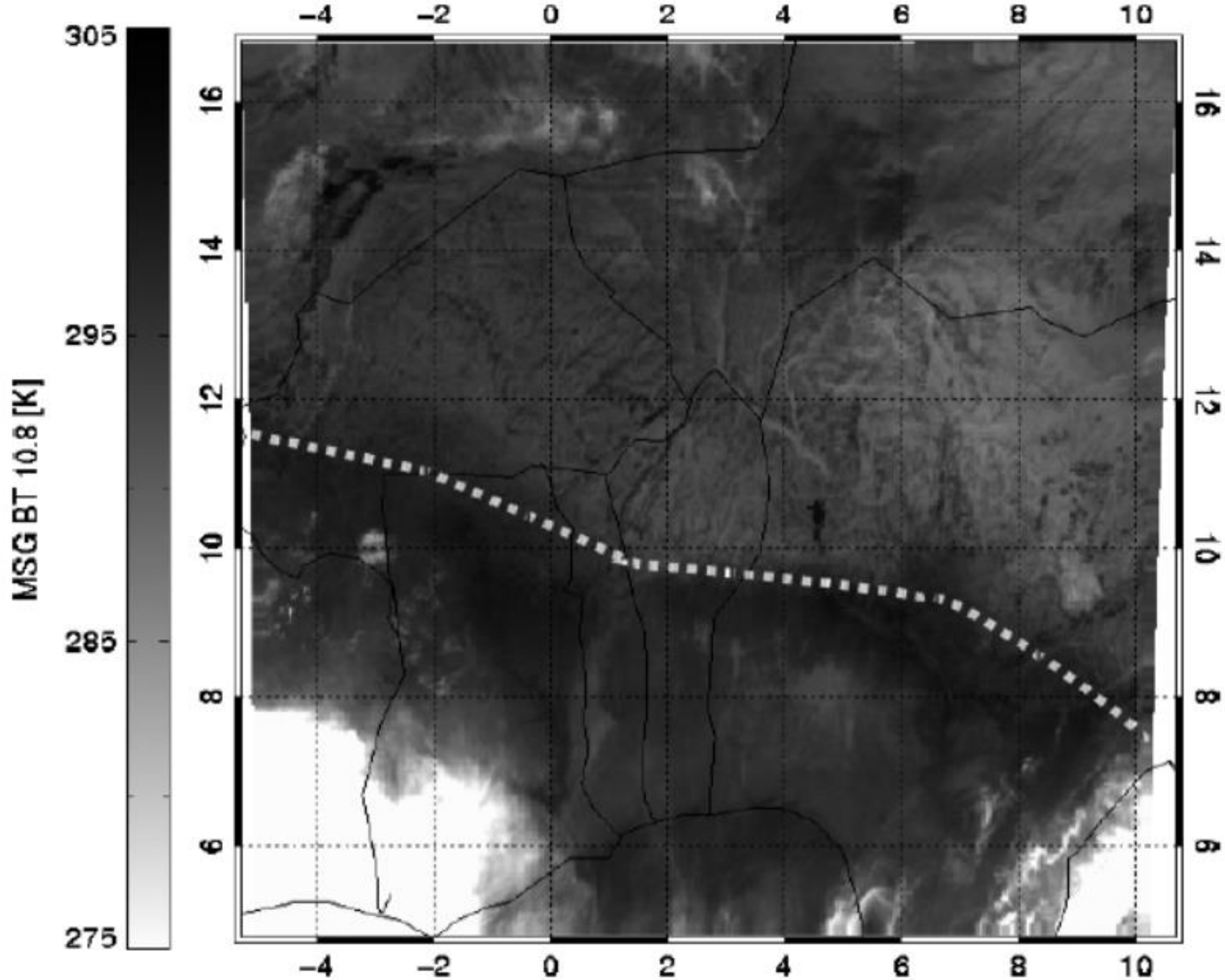

Figure 4.19. MSG SEVIRI 10.8 μm brightness temperature observations from 11 April 2006 at 0200 UTC.
The white dotted line corresponds to the approximate ITD position from model analysis fields, using the 15◦C dew point criterion. From Pospichal et al. (2010).

The ITD is shown here from model data. The satellite observations (independent) show how surface temperature features are clear north of the ITD, but not to the south, where atmospheric humidity reduces the longwave cooling of the surface at night.

African Monsoon Multidisciplinary Analysis

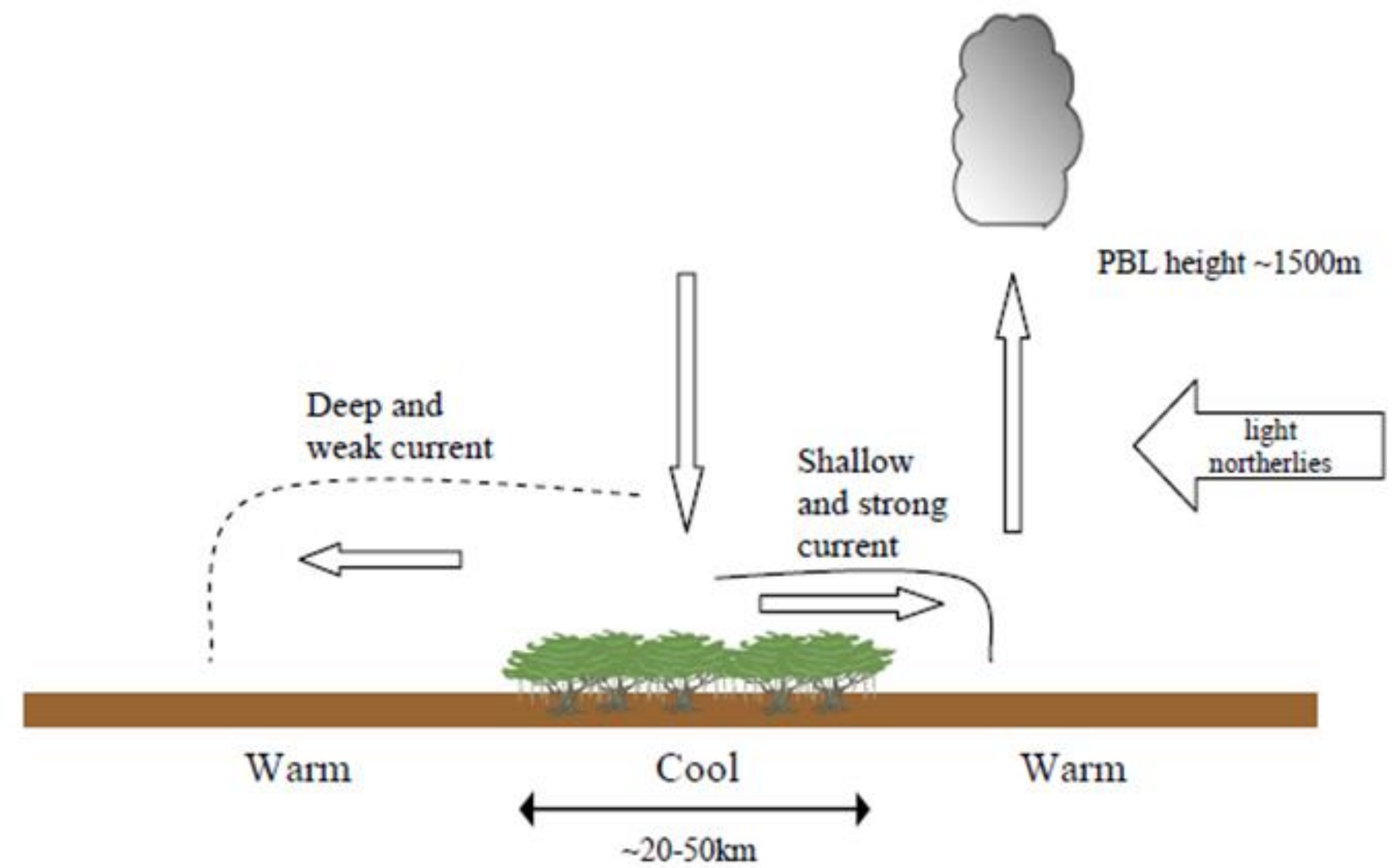

Figure 4.20: Schematic of land-surface influences on temperatures, local winds and local initiation of convection. From Garcia-Carreras et al. (2010).

Chapter 4: *Local Weather* - Lead Author D J Parker

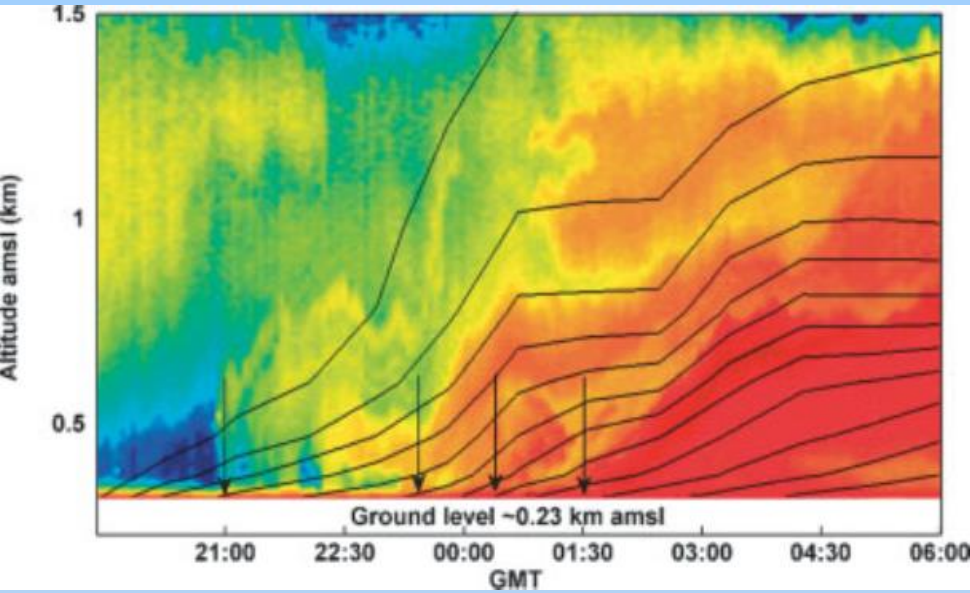

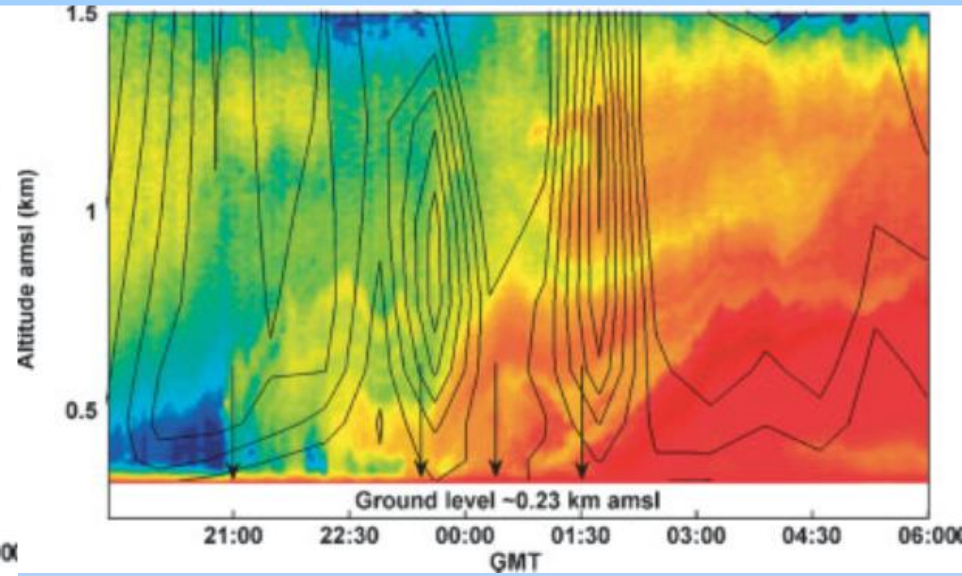

This could be compared with the schematic in Fig 4.14 (in reverse direction).

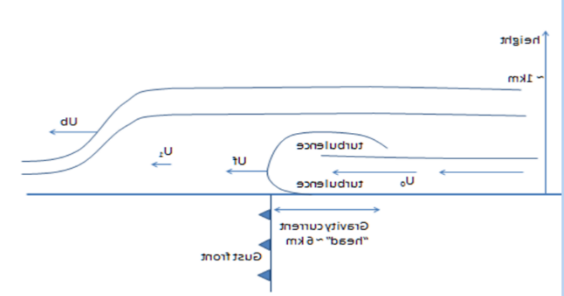

Figure 4.21: Niamey dust data and overlain model potential temperature and vertical velocity fields. Time–height diagram at Niamey Airport for (a) potential temperature (contours with interval 1 ◦C) and (b) vertical velocity (contours with interval 0.5 cms−1), both from a simulation with the Met Office Unified Model at 4 km horizontal resolution. In both, synchronous lidar observations of the dust loading are also shown. Reproduced from Burton et al. (2012).

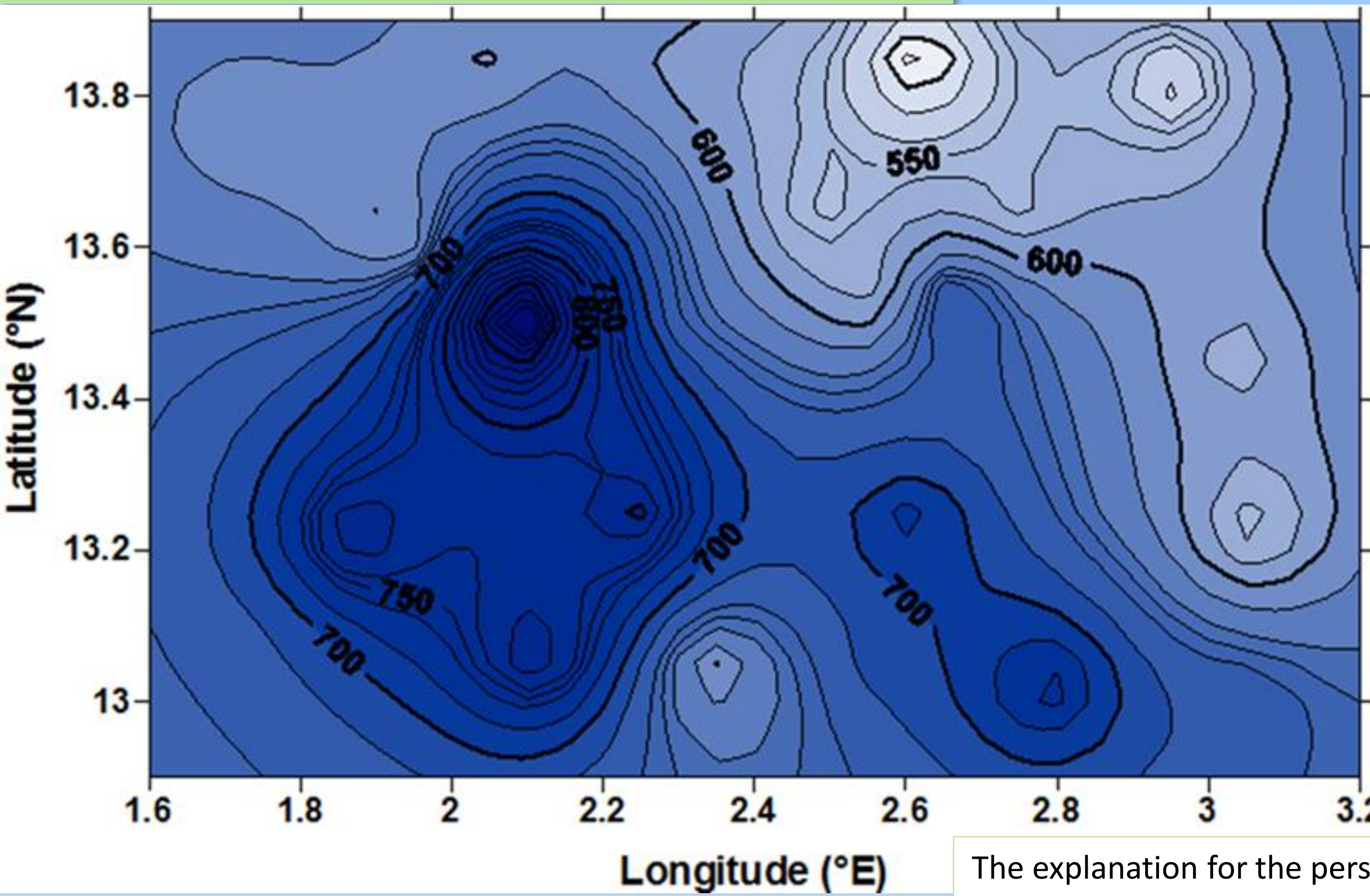

Figure 4.22: Seasonal rainfall totals for 1998 in the vicinity of Niamey.

In parts of the domain there are gradients of 400 mm in seasonal rainfall over a distance of 30 km.
This represents a factor of 2 in seasonal rainfall on the village-to-village scale.
Data collected by the AMMA-CATCH observatory (Lebel et al., 2010).

The explanation for the persistence of such strong rainfall gradients through a rainy season remains a mystery, but it is presumed that a feedback leading to increased rain on wet surfaces is the cause.

African Monsoon Multidisciplinary Analysis

ACMAD

WMO

Chapter 4: *Local Weather* - Lead Author D J Parker

RH / % \ Temperature / °C	27	28	29	30	31	32	33	34	36	37	38	39	40	41	42	43
[illegible]	27	27	28	29	31	33	34	36	38	41	43	46	48	51	54	58
45	27	28	29	31	32	34	36	38	40	43	46	48	51	54	58	
50	27	28	29	31	33	35	37	39	42	45	48	51	55	58		
55	27	29	30	32	34	36	38	41	44	47	51	54	58			
60	28	29	31	33	35	38	41	43	47	51	54	58				
65	28	29	32	34	37	39	42	46	49	53	58					
70	28	30	32	35	38	41	44	48	52	57						
75	29	31	33	36	39	43	47	51	56							
80	29	32	34	38	41	45	49	54								
85	29	32	36	39	43	47	52	57								
90	30	33	37	41	45	50	55									
95	30	34	38	42	47	53										
100	31	35	39	44	49	56										

Table 4.2: Values of heat index (in °C) as a function of 2m temperature (/ °C) and relative humidity (/%)

(http://www.hpc.ncep.noaa.gov/heat_index/about_hi.html and Steadman, 1979).

HI > 39°C: Danger
HI > 51°C: Extreme danger

African Monsoon Multidisciplinary Analysis

Chapter 4: *Local Weather* - Lead Author D J Parker

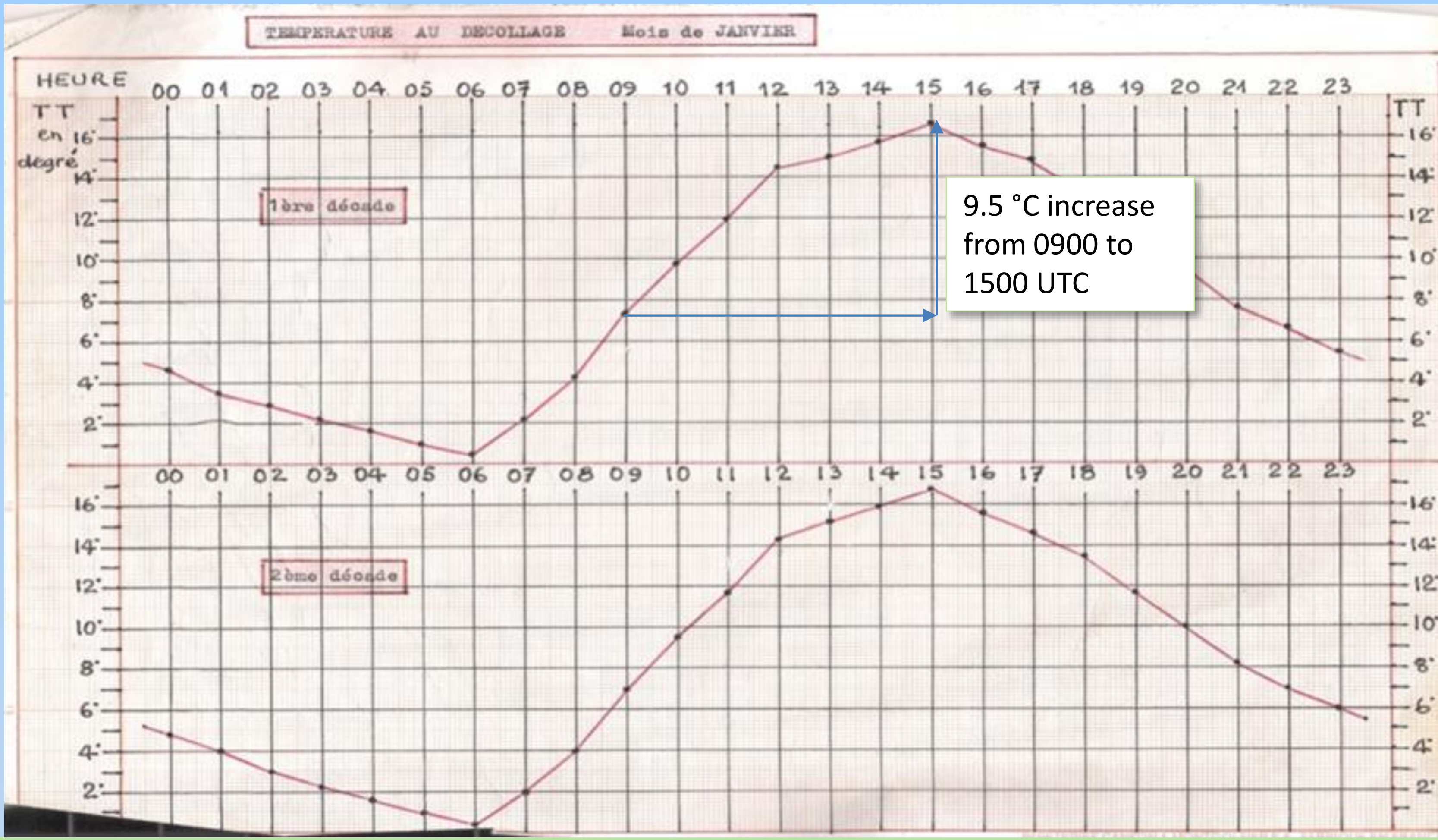

Figure 4.23: Climatological daily variation of surface temperature as used to predict Tn and Tx. This example comes from Niamey in the first decad of January, and is used for the prediction of ambient temperatures for take-off of aircraft. Note that the values are relative, not absolute.

African Monsoon Multidisciplinary Analysis

ACMAD

WMO

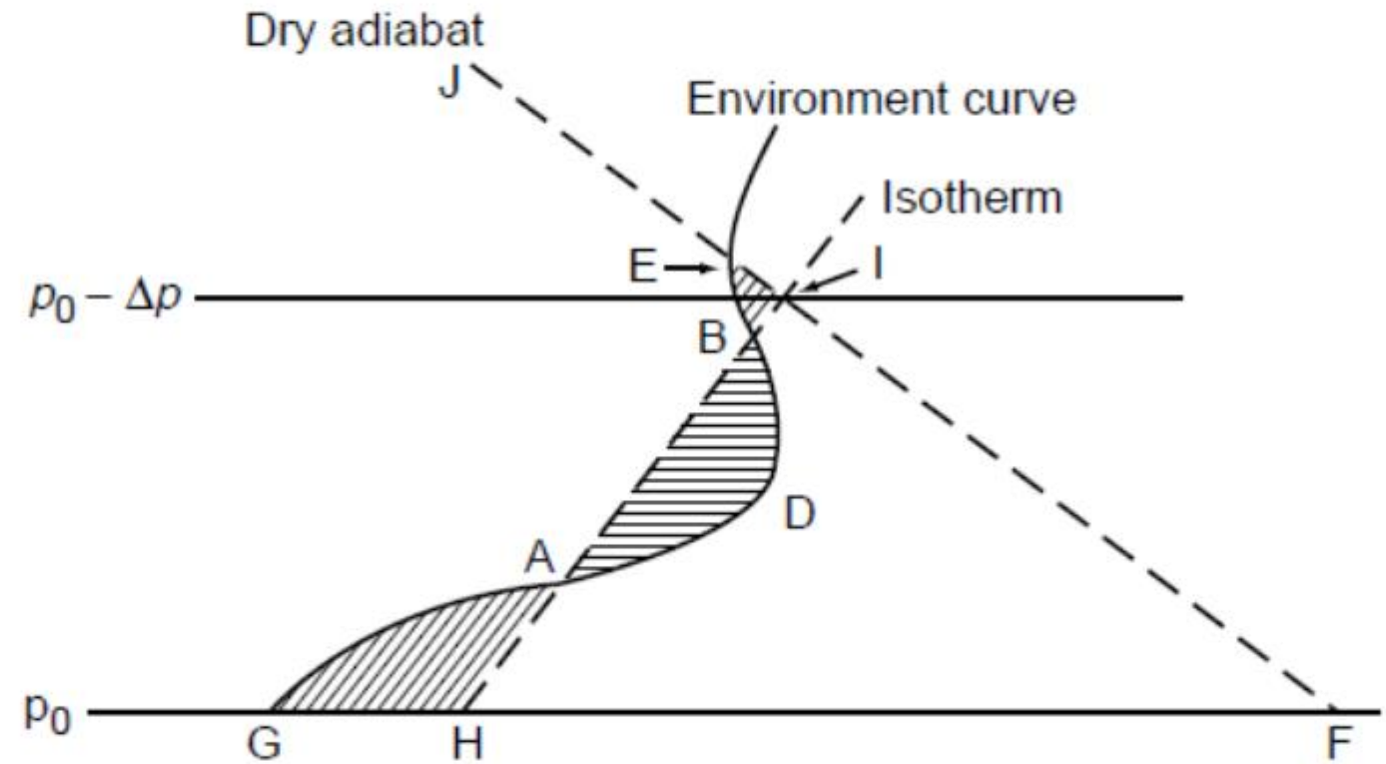

Figure 4.24: Use of a tephigram construction to predict daytime temperatures.
The thickness of the layer, Δp, is found from a lookup table, according to time of year and time of day. The point I is then constructed so that the shaded areas add up to zero (positive and negative areas). F is the forecast surface temperature (Met Office, 1996).

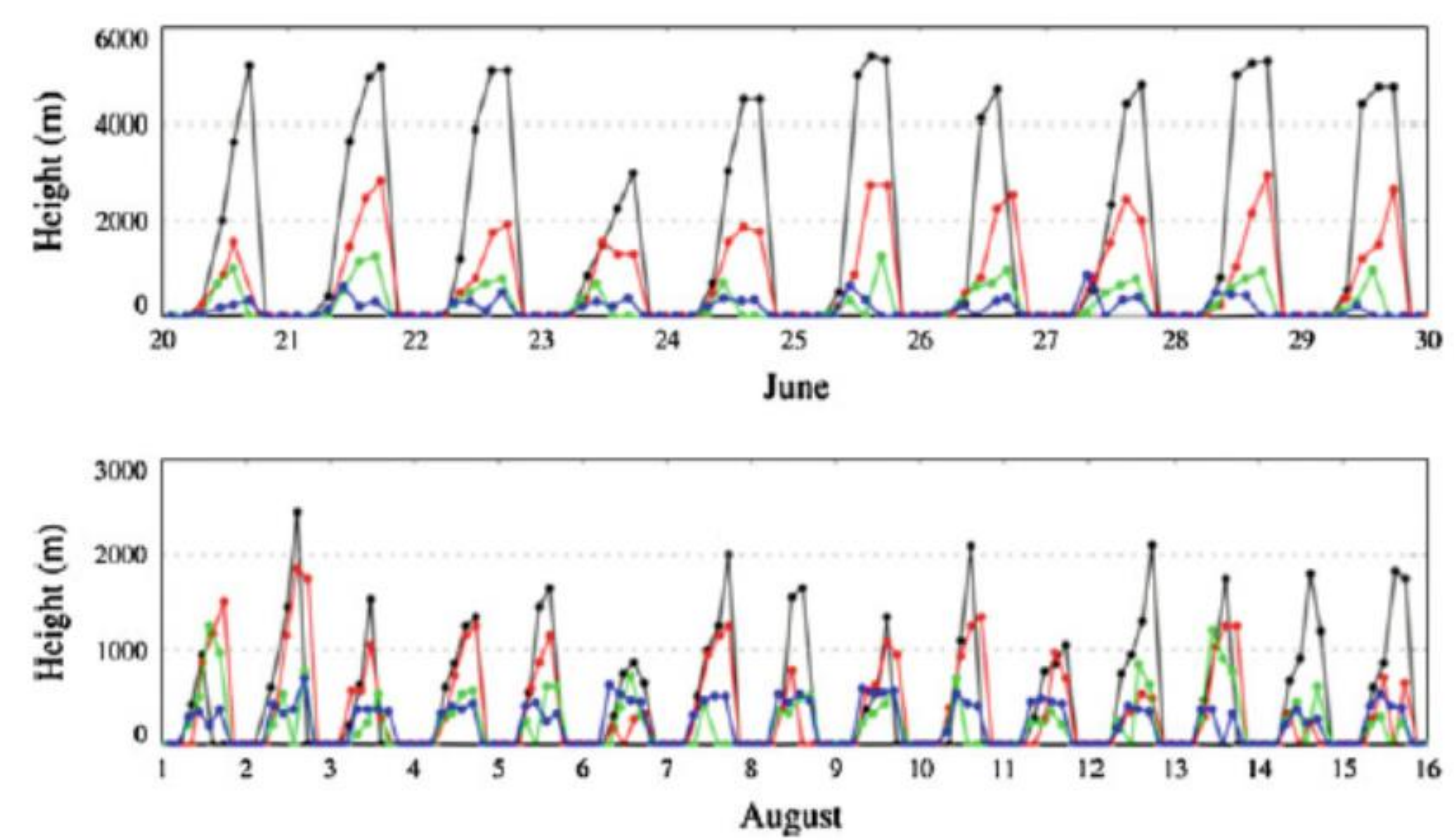

Figure 4.25: Boundary layer depths (/m) for days in the pre-monsoonal period of June, and the monsoonal period of August 2006, from AMMA soundings, for the stations at Agadez (black line, 17°N), Niamey (red line, 13.5°N); Parakou (green line, 9.5°N) and Cotonou (blue line, 6.5°N). From Gounou et al. (2012).

Chapter 4: *Local Weather* - Lead Author D J Parker

Phenomenon (see Section 4.1.2.4)	Effect on minimum temperature, Tn	Effect on maximum temperature, Tx	Comments
Arrival of moist monsoonal air in Sahel	+5 to +10°C		Humid night warmer than dry night
Cu and stratiform cloud: 1–5 okta	+1 to +2°C	−1 to −2°C	
Stratiform cloud: 6–8 okta	+1 to +2°C	−1 to −6°C	Weaker influence in humid air/ Guinea Coast zone. Stronger effect in dry air/over desert
Dust event	+1 to +2°C	up to −3°C	Milton *et al.* (2008). Cold advection also likely to be active
After MCS event	−1 to −2°C	−2 to −4°C	
Strong low-level winds	+1 to +5°C	−1 to −3°C	Stronger nocturnal effect in conditions of clear skies
Soil moisture	Not known	−4 to −8°C	In semi-arid zone
Dense vegetation/ deep-rooted trees	+1 to +2°C	−1 to −2°C	Nocturnal warming in late winter and spring
Topography	−10°C in valleys if cold air pools form under light winds	−1°C per 100 m of altitude	
Urban	−5°C to +2°C	−2°C to +2°C	Highly dependent on vegetation cover of urban and adjacent rural surfaces

Table 4.2: Summary of the effects of various phenomena on daily minimum and maximum temperatures, Tn, Tx, relative to a similar location not influenced by that phenomenon.

Factors involved in fog formation are as follows.

i. Positive pressure tendency, associated with fair weather and clear skies at night, leading to radiation loss.
ii. High RH > 80%. Wet bulb depression: ≤ 2°C.
iii. Surface dry bulb temperature threshold ≤ 23°C.
iv. Light or calm winds overnight.
v. In the coastal region, light onshore winds.
vi. Stable PBL profile; presence of high pressure cells both at surface and 850 hPa level.
vii. Local conditions of surface, e.g. topography or forest cover, modify the likelihood of fog. Forests are a relatively humid environment where fog may be favoured. Fog may also be more likely over hills (hill fog) and in valleys, due to katabatic drainage of cold, humid air downslope.
viii. Soil moisture may also influence fog formation by raising the humidity of the air close to the surface. For example, over Nigeria it is found that fog may follow rain if a ridge forms overnight and the skies clear.

Cloudy conditions (e.g. medium clouds) are counter-productive in relation to fog formation. This is due to the fact that the cloud layers re-radiate the outgoing long wave (terrestrial) radiation back to the Earth's surface, thereby preventing the surface from cooling to the fog-point temperature.

Chapter 4: *Local Weather* - Lead Author D J Parker

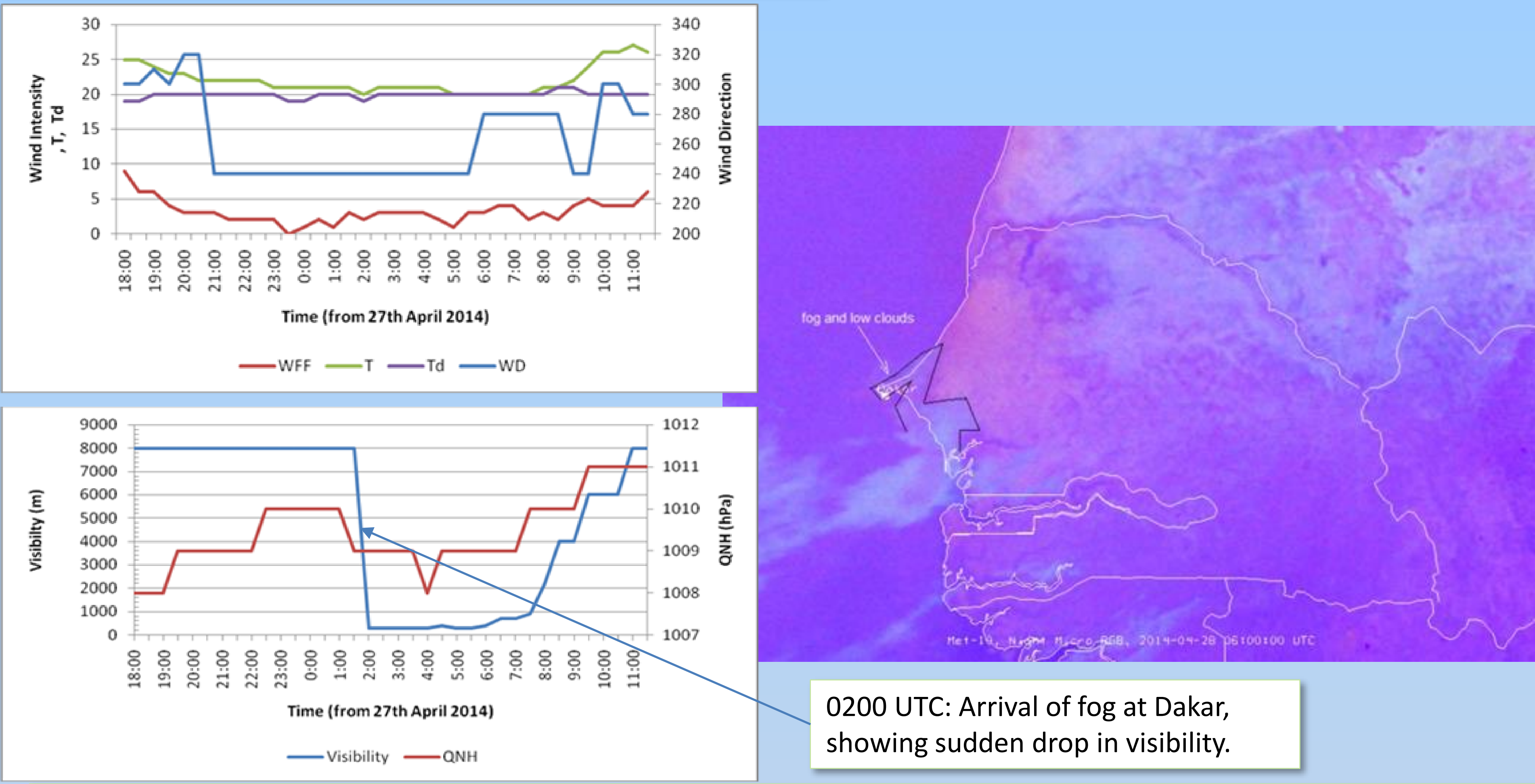

Figure 4.26: Example of coastal fog on the night of 27-28 April 2014 on the coast of Senegal, showing (a)-(b) synoptic measurements from Dakar and (c) RGB night microphysics on 28 April 2014 at 0600 UTC. Details for the RGB image can be found in Section 9.1.4.4 (f). Figure courtesy Jochen Karl Kerkmann, copyright 2015 EUMETSAT.

African Monsoon Multidisciplinary Analysis

ACMAD

WMO

Chapter 4: *Local Weather* - Lead Author D J Parker

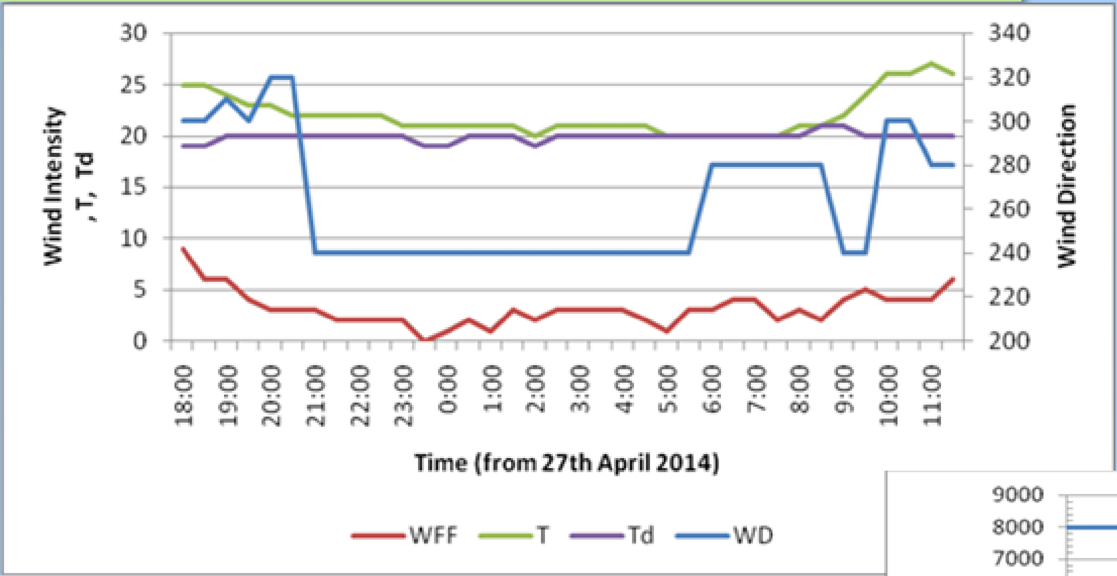

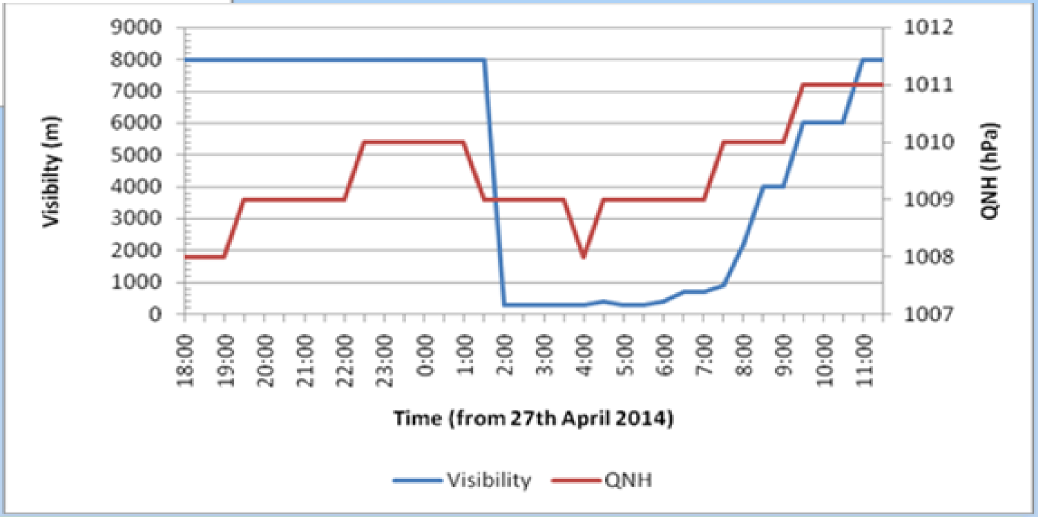

Figure 4.26: Example of coastal fog on the night of 27-28 April 2014 on the coast of Senegal, showing (a)-(b) synoptic measurements from Dakar. Details for the RGB image can be found in Section 9.1.4.4 (f). Figure courtesy Jochen Karl Kerkmann, copyright 2015 EUMETSAT.

African Monsoon Multidisciplinary Analysis

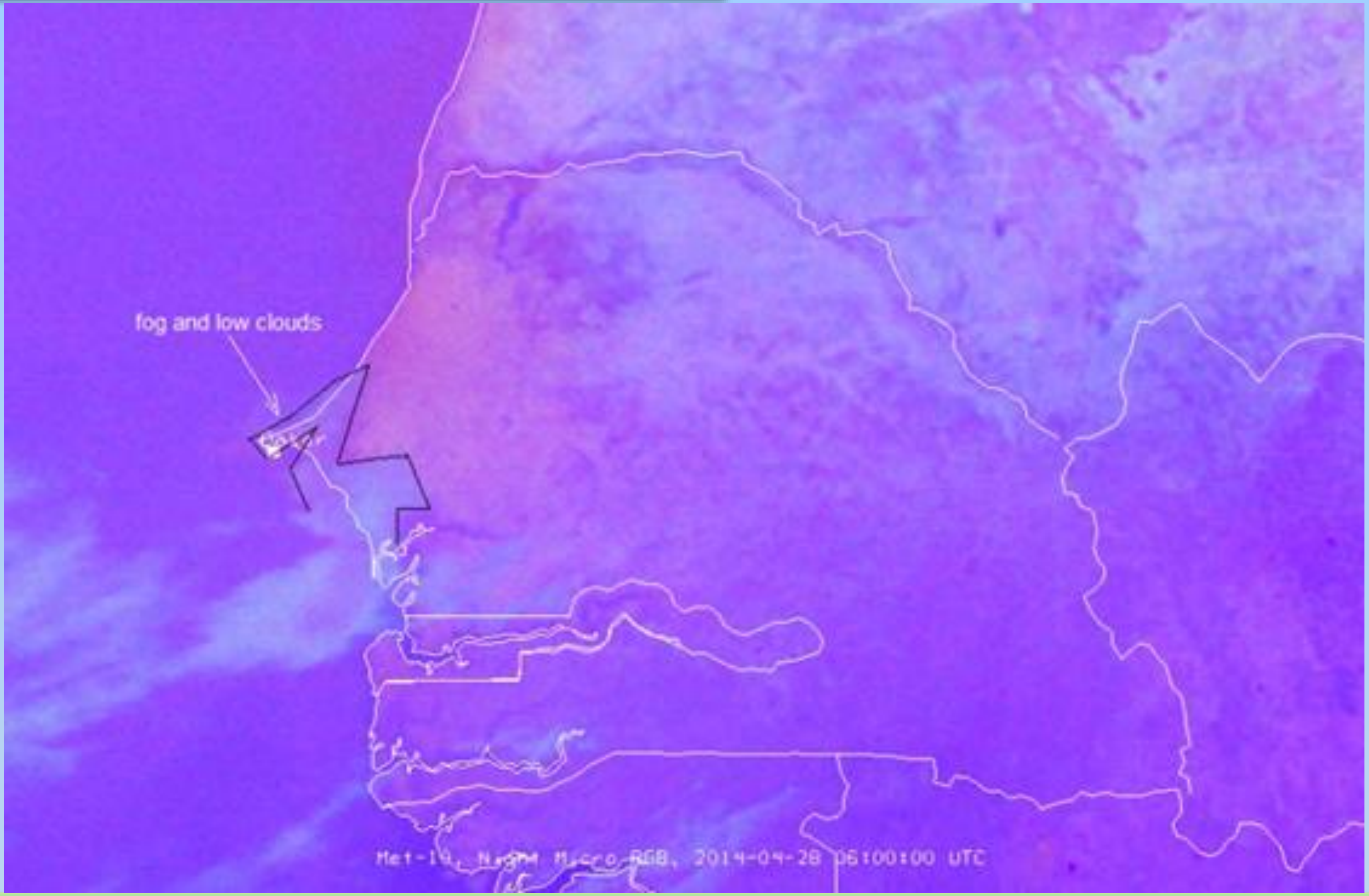

Figure 4.26: Example of coastal fog on the night of 27-28 April 2014 on the coast of Senegal, showing RGB night microphysics on 28 April 2014 at 0600 UTC. Details for the RGB image can be found in Section 9.1.4.4 (f). Figure courtesy Jochen Karl Kerkmann, copyright 2015 EUMETSAT.